Impact of skin effect on single-well push-pull tests with the presence of regional groundwater flow

Xu Li[a], Zhang Wen[a]*, Hongbin Zhan[a,b], Qi Zhu[a]

Manuscript submitted to *Hydrology and Earth System Sciences*

[a]School of Environmental Studies, China University of Geosciences, Wuhan, 430074, China

[b]Department of Geology and Geophysics, Texas A & M University, College Station, TX 77843-3115, USA, Email: zhan@geo.tamu.edu

*Corresponding author: Zhang Wen, Ph.D. Professor. Affiliation: School of Environmental Studies, China University of Geosciences, Wuhan, Hubei, 430074, P. R. China. Email: wenz@cug.edu.cn. Tel: 86-27-67883159. Fax: 86-27-87436235.

Abstract

Single-well push-pull (SWPP) test is one of the most important ways to estimate aquifer transport parameters, e.g. porosity, dispersivity, regional groundwater velocity. The wellbore is surrounded by a finite-thickness skin, such as a gravel pack usually, thus the aquifer can be regarded as a radial two-zone system. If the hydraulic conductivity of the skin is smaller than that of the aquifer formation zone, the skin is defined as a positive one. Otherwise, it is a negative skin. In this study, a numerical model of SWPP test considering skin effects was established using the finite-element COMSOL Multiphysics software to estimate aquifer transport parameters. Several important results were obtained. Firstly, different regional groundwater velocity affects the types of breakthrough curves (BTCs). Secondly, a positive (or negative) skin leads to a slower (or faster) tracer transport process, and a smaller ratio between the hydraulic conductivity of the skin and that of the aquifer formation results in greater solute plume retardation in the skin zone. Thirdly, a larger thickness of the positive skin leads to a higher tracer concentration around the well. The opposite is true if the skin is negative. Besides, different hydraulic conductivities and skin thickness can result in different ratios of tracer mass recovered during the pumping phase. The general conclusion is that the skin effects on SWPP test are significant and should be considered.

Keywords: push-pull test, regional groundwater velocity, solute transport, skin effect

1. Introduction

The single-well push-pull (SWPP) tests have been commonly employed to estimate aquifer parameters, e.g. porosity, dispersivity, biogeochemical reaction rate (Gelhar and Collins, 1971; Hall et al., 1991; Schroth and Istok, 2006; Johnsen et al., 2009). The process of this test can be summarized as follows: A tracer is injected into a target aquifer (injection phase), then the mixed solution is pumped out from the same location (pumping phase). Groundwater samples are taken at regular time intervals at the test well during the pumping process, and parameters can be obtained by fitting the observed breakthrough curves (BTCs) using a proper mathematical model. Conservative or reactive tracers can be utilized, depending on the purpose of the test. In general, conservative tracers have been widely used to estimate regional groundwater flow velocity, porosity, and dispersivity, etc. (Leap and Kaplan, 1988; Haggerty et al., 2001; Hebig-Schubert, 2014). Similarly, one can obtain the information of sorption, cation exchange, microbial processes by applying reactive tracers (Trudell et al., 1986; Field et al., 2000; Tong et al., 2016). For instance, Tong et al. (2016) used SWPP tests to validate the abundant production of hydroxyl radicals due to the oxidization of subsurface sediments.

To interpret the SWPP test results, a proper mathematical model considering the fundamental physical and biogeochemical processes of the test is indispensable (Haggerty et al., 2001; Kleikemper et al., 2002; Schroth and Istok, 2006). From a transport perspective, many existing models are governed by the conventional advection-dispersion equation (ADE), assuming the validity of Fick's law in the SWPP tests (Schroth et al., 2000; Huang et al., 2010). Subsequently, many analytical and numerical solutions of various single-well

models have been developed. For instance, Huang et al. (2010) obtained an exact analytical solution of SWPP test by using Fick's law, considering a partially penetrating well in the aquifer. Besides ADE, a number of non-Fickian transport models of SWPP tests have also been developed in recent years to recognize the influence of media heterogeneity, especially in fractured aquifers (Chen et al., 2017). Such models include multi-rate mass transfer models (Haggerty et al., 2001, Hansen et al., 2016), continuous time random walk (CTRW) (Le Borgne and Gouze, 2008), and fractional advection-dispersion equation (FADE) models (Benson et al., 2004; Chen et al., 2017), to name a few. For instance, Chen et al. (2017) developed a fractional model of multistage SWPP test to simulate non-Fickian behavior for a fractured aquifer. In addition, Schroth et al. (2005) obtained an approximate analytical solution of SWPP test for spherical-flow conditions. Wang et al. (2017) investigated the impacts of transient flow and wellbore storage on SWPP test under transient Forchheimer flow using a finite-difference method.

As mentioned above, SWPP test is a powerful tool for aquifer characterization, but its application for determining the regional groundwater velocity has rarely been discussed in previous studies. The groundwater flow velocity may be measured directly using a two-well tracer test conducted under nature gradient condition, but this requires a monitoring well that is located directly down-gradient at a convenient distance from the test well, which is unlikely in most field applications (as one may not be aware of the hydraulic gradient and groundwater flow direction before the installation of monitoring wells). In fact, in most cases, the hydraulic gradient is determined using a three-well triangle and the groundwater flow velocity (including its magnitude and direction) may be obtained if the hydraulic conductivity

and effective porosity are also known. If the hydraulic conductivity and effective porosity are unavailable, one may rely on the BTCs obtained from such a three-well system in a natural gradient tracer test as an alternative to determine the regional flow velocity and longitudinal and transverse dispersivities as well. This is can be done using the following procedures. First, the direction of hydraulic gradient can be determined based on the hydraulic head measurements in three monitoring wells, and the groundwater flow direction is directly opposite of the hydraulic gradient direction in a horizontally isotropic media (which is usually true for most field applications). Second, after determining the direction of groundwater flow, one has three more parameters to determine: the magnitude of the groundwater flow velocity and longitudinal and transverse dispersivities. Such three unknown parameters can be obtained using the concentrations measured in above three (or more) wells by conducting the natural gradient tracer tests rather than the SWPP tests (Pickens et al., 1981; Michie, 1996; Zimmermann and Huenges, 1999).

However, the natural gradient tracer tests usually take much longer time to complete. This is particularly troublesome when the medium is less permeable, and the regional groundwater flow velocity is relatively small (Schubert et al., 2011). The natural gradient tracer test method is also very costly to implement in deep aquifers as the installation of multiple wells in deep aquifers can be formidably expensive. In contrast, the SWPP test only needs a single well, thus can substantially reduce the cost of test, and becomes a nice alternative for the determination of regional groundwater flow velocity (Leap and Kaplan, 1988; Butler et al., 2009). To serve such a purpose, the SWPP test usually consist of three phases: tracer injection, drift, and pumping, is different from the traditional SWPP test model. The drift

phase allows the injected tracer to drift with regional groundwater velocity, thus it is a key phase to include. Leap and Kaplan (1988) obtained an equation for push-pull test to determine regional groundwater flow velocity in a confined aquifer, and a series of laboratory tests were conducted to verify the accuracy of the model, and they described a "velocity shadow" that exists for some distance downgradient of the well. Hall et al. (1991) considered that if the tracer was not drifted over the "velocity shadow" before pumping, the calculated results of the regional flow velocity would produce a small error with the comparison to the actual value. After that, Monkmeyer and Netzer (1993) in their comment on the paper of Leap and Kaplan (1998), firstly considered a stagnation point (where groundwater velocity is zero) during a SWPP pumping phase, and they considered that the tracer can be recovered, if the tracer was not drifted over stagnation point at the edge of the capture zone. Recently, Charles et al. (2018) conducted a SWPP test in unconfined aquifer, and estimated effective porosity and regional groundwater flow velocity, by using modified equations of Leap and Kaplan (1988).

In addition, the impacts of skin near a pumping well are usually neglected for a SWPP test, which might bring about great errors for the estimation of aquifer parameters and regional groundwater flow velocity. During the process of well implementation, the intrusion of drilling mud into the aquifer in the vicinity of well is inevitable, which can result in the change of the porosity and permeability surrounding the well screen (Hurst et al., 1969). This phenomenon can be regarded as the skin effect (Chen and Chang, 2002; Wang et al., 2012). The thickness of skin usually ranges from a few millimeters to several meters (Novakowski, 1989). The skins can be classified into positive and negative types according to the hydraulic

124 conductivity contrast between the skin and the aquifer formation zone. If the hydraulic
125 conductivity of the skin is smaller than that of the aquifer formation zone, the skin is defined
126 as a positive one. Otherwise, it is a negative skin (Park and Zhan, 2002; Yeh et al., 2003;
127 Wen et al., 2011). Such a skin, regardless of positive or negative, will inevitably alter the
128 flow field near the test well, thus its effect must be taken into consideration for interpreting
129 the SWPP test. For instance, the streamlines of skin zone can converge toward the well in the
130 case of a negative skin, but the opposite is true for a positive skin (Drost et al., 1968;
131 Schubert et al., 2011).

132 In summary, the skin effect is a very important issue from the perspective of SWPP test
133 interpretation. Through a careful check on the literature, we notice that the model of SWPP
134 for estimating groundwater flow velocity needs further investigation, besides, the impacts of
135 skin effects on SWPP tests for estimating groundwater flow velocity have rarely been
136 studied, which will be the purpose of this study. To accomplish the objective, we will
137 investigate a SWPP test containing three phases of injection, rest and pumping using a fully
138 penetrating well. We will use the finite-element COMSOL Multiphysics to numerically
139 simulate the steady-state, two-dimensional (2D) horizontal flow, with specific attention paid
140 to the skin effect.

141 **2. Mathematical model of the SWPP test**

142 To illustrate the problem, we will use a conservative tracer. A confined aquifer is
143 assumed to be unbounded laterally with a uniform regional groundwater flow presented over
144 the entire duration of test. The aquifer is assumed to be homogeneous and horizontally
145 isotropic. A fully penetrating well is used so only the horizontal flow is of concern here. Flow

is assumed to be Darcian and transport is assumed to be Fickian. The test well radius (r_w) is assumed to be sufficiently small so that the wellbore storage is not a concern. The tracer is injected with a constant rate and a constant concentration at the injection phase and is pumped with a constant rate (which could be different from the injection rate) at the pumping phase, after a certain period of drift phase to allow the injected tracer drifting with the regional groundwater flow. The coordinate system is established as follows with the origin at the center of the test well and the *x*-axis pointing to the direction of regional groundwater flow. A 2D schematic diagram investigated here is depicted in Fig.1. The confined aquifer consists of two zones in the radial direction. The first zone, known as the wellbore skin zone, is located around the injection well and has a thickness of r_s-r_w, where r_s is skin radius. The second zone is known as the aquifer formation zone.

2.1 Mathematical model of groundwater flow

Flow of the SWPP test is assumed to be steady-state, thus the groundwater flow velocity of the skin zone can be expressed as the superposition of the flow component generated by the pumping well and the regional flow:

$$\vec{v}_1 = \vec{v}_{r1} + \vec{v}_{x1} \tag{1}$$

$$\vec{v}_{r1} = v_{r1}\vec{e}_r = Q/\left(2\pi\theta_s Br\right)\vec{e}_r \tag{2}$$

$$\vec{v}_{x1} = v_{x1}\vec{e}_x = \left(-K_s J_s/\theta_s\right)\vec{e}_x = \left(v_{d1}/\theta\right)\vec{e}_x \tag{3}$$

$$r = \sqrt{x^2 + y^2} \tag{4}$$

where the arrow over a symbol represents a vector hereinafter; $\vec{v}_{r1}$ is the average radial pore velocity vector of the skin zone generated by the injection (or pumping well) with a magnitude of v_{r1} [L/T]and $\vec{e}_r$ is a unit vector along the radial direction; $\vec{v}_{x1}$ is the regional

groundwater pore flow velocity vector of the skin zone with a magnitude of v_{x1} [L/T] and v_{d1} is the regional groundwater Darcy flow velocity of the skin zone, and $\vec{e}_x$ is a unit vector long the *x*-axis; $\vec{v}_1$ is the lumped groundwater flow velocity in the skin zone [L/T]; *B* is the aquifer thickness [L]; *Q* is the injection or pumping rate [L^3/T], which is positive for the injection and negative for pumping, and *Q* is 0 during the drift phase; K_s is hydraulic conductivity of the skin zone [L/T]; J_s is the hydraulic gradient of regional flow in the skin zone[L/L]; θ_s is the effective porosity of the skin zone [dimensionless], which is assumed to be the same as the total porosity of the aquifer when all the pore spaces are well-connected with negligible immobile porosity; *r* is the radial distance [L] from the well and *x* and *y* are two horizontal coordinates [L], parallel and perpendicular to the regional groundwater flow direction, respectively.

In addition, the groundwater flow velocity in the aquifer formation zone can be expressed as:

$$\vec{v}_2 = \vec{v}_{r2} + \vec{v}_{x2} \tag{5}$$

$$\vec{v}_{r2} = v_{r2}\vec{e}_r = Q/\left(2\pi\theta Br\right)\vec{e}_r \tag{6}$$

$$\vec{v}_{x2} = v_{x2}\vec{e}_x = \left(-KJ/\theta\right)\vec{e}_x = \left(v_{d2}/\theta\right)\vec{e}_x \tag{7}$$

where $\vec{v}_{r2}$ is the average radial pore velocity vector of the aquifer formation zone generated by the injection (or pumping well) with a magnitude of v_{r2} [L/T]; $\vec{v}_{x2}$ is the regional groundwater pore flow velocity vector of the aquifer formation zone with a magnitude of v_{x2} [L/T] and v_{d2} is the regional groundwater Darcy flow velocity of the aquifer formation zone; $\vec{v}_2$ is the lumped groundwater flow velocity in the aquifer formation zone [L/T]; *K* is the

aquifer hydraulic conductivity [L/T]; J is the hydraulic gradient of regional flow in the aquifer formation zone [L/L]; θ is the aquifer effective porosity [dimensionless].

2.2 Mathematical model of solute transport

The solute transport is dominated by advection and dispersion in the two-zone system. The ADE of a conservative solute in the skin zone without source/sink can be written as:

$$\frac{\partial C_1}{\partial t} = \nabla \cdot \left(D \nabla C_1 \right) - \nabla \cdot \left(\vec{v}_1 C_1 \right), \quad r_w < r \le r_s, t > 0 \tag{8}$$

and in the aquifer formation zone as:

$$\frac{\partial C_2}{\partial t} = \nabla \cdot \left(D \nabla C_2 \right) - \nabla \cdot \left(\vec{v}_2 C_2 \right), \quad r_s < r < \infty \tag{9}$$

where C_1 and C_2 are solute concentrations in the skin and aquifer formation zones, respectively [M/L^3]; t is the transport time [T]; D_1 is the hydrodynamic dispersion [L^2/T]; $\nabla \cdot$ and ∇ are the divergence operator and the gradient operator respectively; the hydrodynamic dispersion is a velocity-dependent tensor depicted as:

$$D_{xx} = \frac{\alpha_L v_x^2}{\left| \vec{v} \right|} + \frac{\alpha_T v_y^2}{\left| \vec{v} \right|} + D_{diff} \tag{10}$$

$$D_{yy} = \frac{\alpha_L v_y^2}{\left| \vec{v} \right|} + \frac{\alpha_T v_x^2}{\left| \vec{v} \right|} + D_{diff} \tag{11}$$

$$D_{xy} = D_{yx} = \left(\alpha_L - \alpha_T \right) \frac{v_x v_y}{\left| \vec{v} \right|} \tag{12}$$

$$v = \sqrt{v_x^2 + v_y^2} \tag{13}$$

where D_{xx}, D_{xy}, and D_{yy} are components of the hydrodynamic dispersion coefficient tensor [L^2/T]; D_{diff} is the molecular diffusion coefficient [L^2/T]; α_L is the longitudinal dispersivity [L]; α_T is the transverse dispersivity [L]; the transverse dispersion effect is much smaller, thus

208 one usually assumes $\alpha_L = 10\alpha_T$ (Guvanasen and Guvanasen, 1987; Chen et al., 1999; Chen et

209 al., 2006); v_x is pore velocity in the x direction; v_y is pore velocity in the y direction.

210 **3. Numerical solution of the SWPP test**

211 In this study, a steady-state flow model of 2D horizontal plane was developed based on

212 COMSOL Multiphysics, as shown in Fig. 1. The model region was set to be 40 m × 40 m,

213 and the well has a radius of 0.1 m. In addition, B=10 m, K=8.0 m/d, θ=0.3. According to

214 Fig.1, the boundary conditions for the domain of concern can be expressed as:

215 $$H(x,y)\big|_{s_1} = H_1, \quad H(x,y)\big|_{s_2} = H_2 \tag{14}$$

216 $$K\frac{\partial H}{\partial n}\bigg|_{s_3} = 0, \quad K\frac{\partial H}{\partial n}\bigg|_{s_4} = 0 \tag{15}$$

217 where s_1, s_2 ,s_3 and s_4 are the boundaries of the model; s_1 and s_2 are constant-head boundaries

218 with prescribed total heads of $H_1$and H_2, respectively; both s_3 and s_4 are no-flux boundaries; n

219 is the normal vector of the boundary (an outward pointing vector perpendicular to the

220 boundary). Therefore, a constant regional flow field can be generated and one can obtain

221 different values of v_{x2} by changing the head differences of H_1 and H_2. In this model, constant-

222 head boundaries were prescribed, and the value of H_2 was set as constant 15 m, according to

223 Eq. (7), one can obtain different values of v_{x2} by changing the value of H_1. In the model, a

224 continuous mass flux of injection or pumping rate was assigned at $r=r_w$, which can be

225 expressed as:

226 $$N_0 = \frac{Q\rho}{2\pi r_w B} \tag{16}$$

227 where, N_0 is the mass flux per unit thickness [M/L^2/T]; ρ is the density of groundwater

228 [M/L^3].

A uniform skin near the well was considered in a confined aquifer, and the well skin thickness of r_s-r_w the well skin was assumed to be constant in this model. The skin hydraulic conductivity and effective porosity were set as K_s and θ_s respectively. The default values of the parameters were shown in Table 1.

For the solute model, the initial condition in both the skin and aquifer formation zones are:

$$C_1(r,0) = C_2(r,0) = 0, \ r \geq r_w, \tag{17}$$

During the injection phase, the boundary condition at r=r_w can be described as:

$$C_1(r,t) = C_0, \qquad r = r_w, 0 < t < t_{inj} \tag{18}$$

where C_0 represents the concentration of the injection phase [M/L^3]; t_{inj} is the duration of the injection phase [T]. The third-type boundary condition may also be used to replace the first-type boundary condition of Eq. (20). However, our numerical exercises indicate that both conditions yield nearly the same results except for a very short period of time since the start of injection. Therefore, without loss of generality, we use the first-type boundary condition here as an example to illustrate the methodology.

The concentration and the flux at the interface between the skin and aquifer formation zones are continuous, can be expressed as:

$$C_1(r_s,t) = C_2(r_s,t), \ t > 0 \tag{19}$$

and

$$D\frac{\partial C_1(r_s,t)}{\partial} = D\frac{\partial C_2(r_s,t)}{\partial}, \ t > 0 \tag{20}$$

During the pumping phase, the time-dependent concentration is measured in the borehole. The main target of the test is to obtain several parameters by fitting the observed

BTCs with corresponding theoretical BTCs obtained from a proper analytical or numerical solution. When solute transport through well screen, the boundary condition at the well screen is (Wang et al., 2017):

$$\left.\frac{\partial C}{\partial r}\right|_{r\to r_w^-} = 0 \tag{21}$$

Because the values of velocity and concentration are different around the perimeter of the borehole, it is necessary to integrate the concentration around the borehole with the velocity as the weight to obtain the accurate value of concentration at the well, thus, the flux-averaged concentrations can be expressed as:

$$\overline{C}_{pump} = \frac{\oint_{l_w} v_w C_w}{\oint_{l_w} v_w}, \qquad r = r_w, t_{res} < t < t_{pump} \tag{22}$$

where v_w represents the velocity around the borehole during the pumping [L/T]; C_w represents the concentration around the well perimeter [M/L3]; $\overline{C}$ is the concentration inside the well [M/L3]; l_w is the perimeter of the wellbore [L]. The SWPP test was divided into three phases, the simulation results at the end of each phase, including the hydraulic head and the solute concentration, were set as the initial values for the simulation in the next phase.

The model domain was discretized into 21688 elements, and the mesh size was progressively refined near the well, and the well perimeter was discretized into 28 elements. When the number of element is doubled, the peak solute concentration for the pumping phase varied about 0.17%. Therefore the selected mesh is regarded as sufficiently fine for the problem investigated here. To check the accuracy of the numerical model further, the numerical solution for a special case (without skin) was used to compare with the analytical solution of Huang et al. (2010), who investigated a steady-state flow SWPP model with

injection and extraction phases, without the regional groundwater flow, as shown in Fig.2. The simulated time span of tracer injection and pumping were 0.5 and 1 day, respectively. The other parameters were given as: Q_{inj}= 50 m^3/d, Q_{punp}=-50 m^3/d, B=10 m, α_L=0.1 m, 0.5 m, 1 m, and θ=0.3. C_0 at $r=r_w$ was set as 1.0 mol/m^3. The results showed that our numerical solution agreed perfectly with the analytical solution. For the following analysis, the default values of the parameters are listed in Table 1.

4. Results and discussions

4.1. Types of breakthrough curves for different regional groundwater velocity

The main target of this SWPP test is to estimate the unknown regional groundwater velocity. In order to interpret the BTCs, a parametric study over a wide range of regional groundwater velocities was conducted. Fig. 3 shows the BTCs for the pumping phase with different regional groundwater velocities, like 5×10^{-7} m/s, 1×10^{-6} m/s, 1.5×10^{-6}m/s, 2×10^{-6} m/s, 2.5×10^{-6} and 3×10^{-6} m/s. Besides, α_L =0.1 m, Q_{inj}= 30 m^3/d, Q_{pump}=-15 m^3/d, and the other parameters are the same as those used in Table 1. It is found that different regional groundwater velocities have great impacts on BTCs, and such impacts depend on the value of the regional groundwater velocities. It is found that the tracer concentration is smaller at early stage with a greater regional groundwater velocity. Additionally, it is notable that a larger regional groundwater velocity will result in a longer tailing.

Fig. 4 shows the superposition of flow components generated by the pumping well and the regional flow. A minor point to note is that Figure 4 only shows a flow pattern for a small area nearby the well, not for the entire domain, thus the streamlines there appear not orthogonal to the upper and lower boundaries. For the pumping phase, one can see that there

294 is a stagnation point (Sp), where the groundwater velocity (v_2) is zero, located at the dividing
295 streamline (Ds) or envelope of the capture zone as shown in Fig.4. The Ds divides the flow
296 into the capture zone and the non-capture zone, while the Sp represents the uppermost
297 location downgradient from the pumping well inside a capture zone. If the tracer does not
298 drift beyond the stagnation point of the capture zone during the drift phase, it can be extracted
299 from the aquifer, which acts like a fishing net to collect all the products together. Therefore,
300 different convergence situations of tracer due to variable dividing streamlines result in a
301 series of BTC types. In order to interpret this behavior explicitly, the concentration
302 distributions in a 2D horizontal plane at t_{pump}=0 hr with different regional groundwater
303 velocities are shown in Fig. 5. One can see that a certain amount of tracer mass may be
304 retained near the symmetry axis (x-axis) and around the well when the regional groundwater
305 velocity is relatively low, such as $v_d=1\times10^{-6}$ m/s and 1.5×10^{-6} m/s, as shown in Figs.5a-5b,
306 resulting in relatively high concentrations in the wellbore at early stage. On the contrary, a
307 larger regional groundwater velocity leads to a faster tracer transport process, causing the
308 tracer mass drifting away from the well, as shown in Figs.5c-5d. Besides, one can also see
309 that a larger regional groundwater velocity leads to a smaller distance from Sp to well,
310 resulting in a smaller portion of tracer mass that can be extracted during the pumping phase.
311 The opposite is true for the case of a smaller regional groundwater velocity. For instance, as
312 for the tracer mass on the left side of the dividing streamline, they can be extracted by smaller
313 velocities such as $v_d=5\times10^{-7}$ m/s and 1×10^{-6} m/s, as shown in Figs.5a-5b, but very limited
314 tracer can be captured with larger velocities like $v_d=3\times10^{-6}$ m/s. And this further confirms
315 the reasonability of the BTC types in Fig. 3. In addition, the effects of the duration of the rest

316 phase, porosity and dispersivity on BTCs have been analyzed in a supplementary material as
317 references.

318 **4.2. The effects of skin hydraulic conductivity on BTCs in the SWPP test**

319 As mentioned above, the well skin includes two general types, i.e., a positive skin or a
320 negative skin. Denoting the hydraulic conductivities of skin and aquifer (or aquifer formation
321 zone) respectively as K_s and K, one can use a new parameter $\delta=K_s/K$ to reflect the skin
322 impact, where δ is a parameter reflecting the type of the skin and called the "skin index"
323 hereinafter. Specifically, $\delta<1$ represents a positive skin, while $\delta>1$ represents a negative skin.
324 Note that the case of $\delta=1$ represents the case without a skin. In this section, we will provide a
325 detailed analysis on the impact of the skin hydraulic conductivity on SWPP test.

326 Fig. 6 shows the effect of different skin indexes on BTCs during the pumping phase.
327 The parameters are given as: $v_d=3\times10^{-6}$ m/s, Q_{inj}=30 m^3/d, Q_{pump}=-30 m^3/d, α_L=0.1 m, r_s=0.7
328 m, δ= 0.25, 0.5, 1, 1.5 and 2, respectively. The results indicate that the concentration gets
329 higher at early stage of pumping when the skin index is lower, as shown in Fig. 6. This may
330 be explained as follows. A skin with a lower δ value (or a lower permeability value in respect
331 to that of the formation) essentially serves as a somewhat "shield" around the test well that
332 can make the spreading of the tracer mass out of the test well more difficult during the
333 injection phase. Consequently, more tracer mass will be retained near the test well either in
334 the skin or near the skin. Therefore, during the pumping phase of the test, more tracer mass
335 can be extracted during the early stage of the pumping phase, leading to higher concentration
336 during that stage. The facts are just the opposite for a larger δ value, this is because a negative
337 skin ($\delta>1$) is somewhat like a "high conductance zone" rather than a "shield", and can

338 facilitate the spreading of tracer mass away from the test well during the injection phase.
339 Therefore, less tracer mass will be retained near the test well for a higher skin index, thus less
340 concentration will be seen during the early stage of pumping in the wellbore.

341 To further explicitly interpret this behavior, the concentration distributions in a 2D
342 horizontal plane at t_{pump}=0 hr with different δ values are shown in Fig. 7. As can be seen in
343 Fig.7, a lower δ value (or a lower skin hydraulic conductivity) leads to more tracer
344 accumulation in the skin zone after the drift phase. On the contrary, it is quite obvious to see
345 that a larger δ value (or a larger skin hydraulic conductivity) leads to a less tracer
346 concentration in the skin zone at the early stage of the pumping phase. For instance, we can
347 see that tracer accumulation in the skin zone for the cases of δ=2 is clearly less than the cases
348 of δ=0.5 and 0.25.

349 Fig. 8 displays the curves of concentration versus distance at t_{pump}=0 hr with δ= 0.25,
350 0.5, 1, 1.5 and 2, respectively. We can see that the concentration gets higher in the skin zone
351 when the skin index δ is lower, as shown in Fig. 8. The results indicate that a lower skin
352 hydraulic conductivity leads to more tracer accumulation in the skin zone after the drift
353 phase. The opposite is true if the skin index δ is larger. In addition, we can see that the peak
354 of solute transport shorter distances at corresponding times with a lower δ value, results in the
355 concentration gets higher at early stage of pumping as shown in Fig. 6. Therefore, the
356 presence of the skin zone will lead to the variations of the concentration curves versus
357 distance in the aquifer system.

358 **4.3. Effects of skin thickness on BTCs in the SWPP test**

In this section, we will analyze the impacts of the skin thickness on BTCs. The parameters are given as: v_d=3×10^{-6} m/s, Q_{inj}= 30 m^3/d, Q_{ext}=-30 m^3/d, δ= 0.5 (positive skin), δ= 2 (negative skin), α_L=0.1 m, and r_s= 0, 0.3, and 0.7 m, respectively. For the case of δ= 0.5 (positive skin), one can see that the concentration gets higher at early stage with the increase of r_s in Fig. 9. The explanation is similar to that for Fig. 6, as a thicker positive skin means a thicker "shield" surrounding the test well, preventing the injected tracer mass from spreading further away from the test well, thus leading to higher concentrations during the early stage of the extraction phase. While for the case of δ= 2 (negative skin), it can be found that the concentration shows a decreasing trend with the increase of r_s, as a thicker negative skin means a thicker high conductance zone surrounding the test well, which will facilitate the spreading of injected tracer mass further away from the test well.

To further explicitly interpret this behavior, the concentration distributions in a 2D horizontal plane at t_{pump}=0 hr with different positive (or negative) skin thickness are shown in Fig. 10. It is evident that a larger positive skin thickness leads to more tracer accumulation in the skin zone after the drift phase. While for the case of negative skin, one can see that a greater portion of tracer mass migrates away from the test well after the cease of injection with a greater r_s in Fig. 10. For instance, one can see that tracer accumulation in the skin zone for the cases of r_s=0.7 and δ=2 is clearly less than the case of r_s=0.7 and δ=0.5.

Fig. 11 displays the curves of concentration versus distance at t_{pump}=0 hr with δ= 0.5 (positive skin), δ= 2 (negative skin), r_s= 0, 0.3, and 0.7 m, respectively. For the case of δ= 0.5 (positive skin), one can see that the concentration gets higher in the skin zone when r_s is larger, as shown in Fig. 11. The results indicate that a thicker skin leads to more tracer

accumulation in the skin zone after the drift phase for a lower skin hydraulic conductivity. The facts are just the opposite for the case of negative skin. In addition, one can see that the peak of solute for a positive skin transport shorter distances at corresponding times with a thicker skin, results in the concentration gets higher at early stage of pumping as shown in Fig. 9. While for the case of a negative skin, the peak of solute transport longer distances with a thicker skin. Therefore, different skin properties (skin type and thickness) will result in different shapes of BTCs in Fig.9.

4.4 Recovered tracer mass estimations

To allow for a more quantitative comparison between simulations, we have computed the ratio of tracer mass recovered at the end of each SWPP test for different skin properties (skin type and thickness). Such a ratio can be can be written as:

$$\mu = \frac{m_{pump}}{m_{inj}} = \frac{\int_0^{t_{pump}} Q_{pump} \overline{C}_{pump} dt}{Q_{inj} t_{inj} C_0} \tag{26}$$

where, m_{inj} is the tracer mass injected during the injecting phase [M]; m_{pump} is the tracer mass recovered during the pumping phase [M]; μ is the percentage of recovered tracer mass in the injecting tracer mass [dimensionless].

According to Fig. 9, the value the tracer concentration recovered was integrated from t_{pump} =0 to 48 hr, then we can obtain the tracer mass recovered for different skin properties, e.g. δ= 0.5 (positive skin), δ= 2 (negative skin), and r_s= 0, 0.2, and 0.6 m, respectively. Table 2 shows the percentage of recovered tracer mass in the injecting tracer mass for different skin properties. The results indicate that a lower δ value (or a lower permeability value in respect to that of the aquifer formation) leads to a larger ratio of tracer mass recovery. In addition, for the case of a positive skin, a larger r_s leads to larger ratio of tracer mass recovery, while the

opposite is true for the case of a negative skin. In short, the skin properties (skin type and thickness) can result in different tracer mass recovery ratios.

4.5. Parameter estimations

As discussed in the above sections, the difference between the BTCs of the SWPP test under a skin and a non-skin is obvious. From a practical standpoint, hydrogeologists are interested in the accuracy of parameter estimation based on SWPP models, however, the phenomenon of skin effect is inevitable. Therefore, in the following, we will analyze how the skin effect affects the estimation of aquifer properties such as dispersivity, porosity and regional groundwater flow velocity, and the SWPP model with skin effect is chosen as the reference.

Now an interesting question is: what is the consequence if one adopts the non-skin SWPP model to interpret BTCs obtained from the model with skin? In another word, how different are the estimated parameters (e.g. dispersivity, porosity and regional groundwater velocity) applying the non-skin SWPP model from their ‘‘actual” values based on the SWPP model with skin? If the differences between estimated and ‘‘actual” parameter values are not negligible, one can conclude that the skin effect should be taken into consideration when using the SWPP test model to estimate parameters. Fig. 12 shows BTCs at the well fitted by the non-skin model for different skin types (a positive skin or a negative skin). The “actual” parameters used in the SWPP model with skin are set as: v_d=3×10^{-6} m/s, Q_{inj}= 30 m^3/d, Q_{ext}=-30 m^3/d, δ= 0.5 (positive skin), δ= 2 (negative skin), α_L=0.1 m, θ =0.3 and r_s= 0.7 m, respectively. The circle lines are created by the numerical solution of the SWPP test with skin in three phases. The dashed lines are created by the non-skin SWPP test model. Using the

425 trial-and-error method, we find that it is difficult to fit BTCs at the early stage of the SWPP
426 test for a positive skin, but the fitness is good for a negative skin as shown in Fig. 12. Table 3
427 shows the parameter estimated by the non-skin model. One can see that for the case of a
428 positive skin, both groundwater flow velocity and porosity estimated are smaller than their
429 real values, and longitudinal dispersivity is larger than the real value based on the model with
430 skin. In addition, for the case of a negative skin, groundwater flow velocity, porosity and
431 longitudinal dispersivity estimated are larger than their real values based on the model with
432 skin. In summary, the parameters estimated by the non-skin model are considerable different
433 from the real values, results in larger errors in parameter estimation if the non-skin model is
434 mistakenly used when the skin presents.

435 **5. Conclusions**

436 In this study, a numerical model for a SWPP test with the presence of a regional
437 groundwater flow field, considering both the positive and negative skin effects was
438 investigated. There is a strong interaction between regional groundwater flow and well flow,
439 and various types of BTCs were analyzed for different regional groundwater velocity during
440 pumping phase. Besides, the numerical model of SWPP test can offer a way to estimate
441 unknown parameters: i.e., regional groundwater velocity, effective porosity, and dispersivity
442 by fitting to the observed BTCs. The effects of both the hydraulic conductivities and
443 thickness of the skin zone on BTCs had also been considered. The following conclusions can
444 be drawn:

445 1. Regional groundwater velocity has a significant effect on the shape of BTCs, a lower
446 regional groundwater velocity means that more tracer can be accumulated near the

symmetry plane around the well. The opposite is true for a case of a larger regional flow velocity, resulting in a longer tailing of BTCs obtained during the extraction phase. In addition, the pattern and location of the dividing streamline determine the quantity of tracer mass extracted during the pumping phase.

2. A lager skin index results in a lower concentration for BTCs at early stage of pumping. On the contrary, a smaller skin index means a higher concentration for BTCs. A lager thickness of a positive skin leads to a larger concentration of tracer near the symmetry plane around the well, and the opposite is true for the case of a negative skin. In addition, a smaller skin index means that solute plume can accumulate more in the skin zone, otherwise, a larger skin index results in a solute plume drifting further away from the skin zone after the cease of the injection phase.

3. The non-skin SWPP test model is used to interpret BTCs obtained from the model with skin, and the estimated parameters are very different from the ‘‘actual” values, results in larger errors in parameter estimation if the non-skin model is mistakenly used when the skin presents . Therefore, the impact of skin effect near a pumping well should not be neglected for SWPP tests.

Acknowledgements

This research was partially supported by the National Natural Science Foundation of China (Grant Numbers: 41772259, 41372253, 41521001), the Natural Science Foundation of Hubei Province, China (2018CFA085，2018CFA028), the Fundamental Research Funds for the Central Universities, China University of Geosciences (Wuhan). We appreciate the

comments raised by three anonymous reviewers and the Editor, which help us improve the quality of the paper substantially.

References

Benson, D. A., Tadjeran, C., Meerschaert, M. M., Farnham, I., and Pohll, G.: Radial fractional-order dispersion through fractured rock, Water Resour. Res., 40(12), 87-87, 2004.

Butler, A.P., Mathias, S.A., Gallagher, A.J., Peach, D.W., and Williams, A.T.: Analysis of flow processes in fractured chalk under pumped and ambient conditions (UK), Hydrogeol J., 17(8), 1849-1858, 2009.

Chen, C. S., and Chang, C. C.: Use of cumulative volume of constant-head injection test to estimate aquifer parameters with skin effects: Field experiment and data analysis, Water Resour. Res., 38(5), 189-195, 2002.

Chen, J. S., Chen, C. S., Gau, H. S., and Liu, C. W.: A two-well method to evaluate transverse dispersivity for tracer tests in a radially convergent flow field, J. Hydrol., 223(3-4), 175-197, 1999.

Chen, K.W., Zhan, H.B., and Yang, Q: Fractional models simulating non-fickian behavior in four-stage single-well push-pull tests, Water Resour. Res., 53(11), 9528-9545, 2017.

Drost, W., Klotz, D., Koch, A., Moser, H., Neumaier, F., and Rauert, W: Point dilution methods of investigating ground water flow by means of radioisotopes, Water Resour. Res., 4(1), 125-146, 1968.

Field, J. A., Sawyer, T. E., Schroth, M. H., Humphrey, M. D., and Istok, J. D.: Effect of cation exchange on surfactant-enhanced solubilization of trichloroethene, J. Contam. Hydrol., 46(1-2), 131-149, 2000.

492 Gelhar, L. W., and Collins, M. A.: General analysis of longitudinal dispersion in nonuniform
493 flow. Water Resour. Res., 7(6), 1511-1521, 1971.
494 Guvanasen V., and Guvanasen V M.: An approximate semianalytical solution for tracer
495 injection tests in a confined aquifer with a radially converging flow field and finite
496 volume of tracer and chase fluid, Water Resour. Res., 23(8), 1607-1619, 1987.
497 Haggerty, R., Fleming, S. W., Meigs, L. C., and McKenna, S.A.: Tracer tests in a fractured
498 dolomite: 2. Analysis of mass transfer in single-well injection-withdrawal tests, Water
499 Resour. Res., 37(5), 1129-1142, 2001.
500 Hall, S.H., Luttrell, S.P., and Cronin, W.E.: A method for estimating effective porosity and
501 ground-water velocity, Ground Water., 29(2), 171-174, 1991.
502 Hansen, S. K., Berkowitz, B., Vesselinov, V. V., O'Malley, D., and Karra, S. Push-pull tracer
503 tests: their information content and use for characterizing non-fickian, mobile-immobile
504 behavior, Water Resour. Res., 52(12), 9565-9585, 2016.
505 Hebig-Schubert, K.: Deep groundwater flow systems and their characterization in single-well
506 settings by "push-pull" tracer tests, Int. J. Fatigue., 15(5), 441, 2014.
507 Huang, J. Q., Christ, J. A., and Goltz, M. N.: Analytical solutions for efficient interpretation
508 of single-well push-pull tracer tests, Water Resour. Res., 46(8), 863-863, 2010.
509 Hurst, W., Clark, J. D., and Brauer, E. B.: Skin effect in producing wells, J. Petrol. Technol.,
510 21(11), 1483-1489, 1969.
511 Kleikemper, J., Pelz, O., Schroth, M. H., and Zeyer, J.: Sulfate-reducing bacterial community
512 response to carbon source amendments in contaminated aquifer microcosms, Fems
513 Microbiol Ecol., 42(1), 109-118, 2002.

514 Johnsen, S. G., Whitson, C. H.: Analytical treatment of a push-pull “echo” test. Transp.
515 Porous Media, 77(3), 399. 2009.
516 Leap, D. I., Kaplan, P. G.: A single-well tracing method for estimating regional advective
517 velocity in a confined aquifer: Theory and preliminary laboratory verification. Water
518 Resour. Res., 24(7), 993-998, 1988.
519 Le Borgne, T., and Gouze, P.: Non-Fickian dispersion in porous media: 2. Model validation
520 from measurements at different scales, Water Resour. Res., 44(6), 2389-2393, 2008.
521 Michie, U.: The geological framework of the sellafield area and its relationship to
522 hydrogeology, Q. J. Eng. Geol., Hydroge. 29(Supplement_1), S13-S27, 1996.
523 Novakowski, K. S.: A composite analytical model for analysis of pumping tests affected by
524 well bore storage and finite thickness skin, Water Resour. Res., 25(9), 1937-1946, 1989.
525 Park, E. and Zhan, H. B.: Hydraulics of a finite-diameter horizontal well with wellbore
526 storage and skin effect, Adv. Water Resour., 25(4), 389-400, 2002.
527 Pickens, J. F., Jackson, R. E., Inch, K. J., and Merritt, W. F.: Measurement of distribution
528 coefficients using a radial injection dual-tracer test, Water Resour. Res., 17(3), 529-544,
529 1981.
530 Paradis, C. J., Mckay, L. D., Perfect, E., Istok, J. D., and Hazen, T. C.: Push-pull tests for
531 estimating effective porosity: expanded analytical solution and in situ application.
532 Hydrogeol J 26(3), 1-13, 2018.Schroth, M. H., Istok, J. D., and Haggerty, R.: In situ
533 evaluation of solute retardation using ingle-well push-pull tests, Adv. Water Resour.,
534 24(1), 105-117, 2001.

535 Schroth, M. H. and Istok, J. D.: Models to determine first-order rate coefficients from single-
536 well push-pull tests, Ground Water., 44(2), 275-283, 2006.
537 Schroth, M. H., and Istok, J. D.: Approximate solution for solute transport during spherical-
538 flow push-pull tests, Ground Water., 43(2), 280-284, 2005.
539 Schubert, M., Brueggemann, L., Knoeller, K., and Schirmer, M.: Using radon as an
540 environmental tracer for estimating groundwater flow velocities in single-well tests,
541 Water Resour. Res., 47(3), 944-956, 2011.
542 Tong, M., Yuan, S., Ma, S., Jin, M., Liu, D., Cheng, D., and Wang, Y.: Production of
543 abundant hydroxyl radicals from oxygenation of subsurface sediments, Environ. Sci.
544 Technol., 50(1), 214-221, 2016.
545 Trudell, M. R., Gillham, R. W., and Cherry, J. A.: An in-situ study of the occurrence and rate
546 of denitrification in a shallow unconfined sand aquifer, J. Hydrol., 83(3), 251-268, 1986.
547 Wang, C. T., Yeh, H. D., and Tsai, C. S.: Transient drawdown solution for a constant
548 pumping test in finite two-zone confined aquifers, Hydrol. Earth Syst. Sci. Discuss.,
549 16(2), 441-449, 2012.
550 Wang, Q., Zhan, H., and Wang, Y.: Single-well push-pull test in transient forchheimer flow
551 field, J. Hydrol., 549, 125-132, 2017.
552 Wen, Z., Zhan, H. B., Huang, G. H., and Jin, M. G.: Constant-head test in a leaky aquifer
553 with a finite-thickness skin, J. Hydrol., 399(3-4), 326-334, 2011.
554 Yeh, H. D., Yang, S. Y., and Peng, H. Y.: A new closed-form solution for a radial two-layer
555 drawdown equation for groundwater under constant-flux pumping in a finite-radius well,
556 Adv. Water Resour., 26(7), 747-757, 2003.

557 Zimmermann, G., and Huenges, E.: Rock permeability and fluid pressure at the KTB.
558 implications from laboratory-and drill hole-measurements, Oil. Gas. Sci. Technol.,
559 54(6), 689-694, 1999.

Figure Captions:

Fig.1 The schematic diagram of the flow system. s_1, s_2, s_3 and s_4 are the boundaries of the model, and s_1 and s_2 are constant-head boundaries; both s_3 and s_4 are no-flux boundaries;

Fig.2 Comparison between the numerical solutions of this study and the analytical solutions of Huang et al. (2010).

Fig.3 BTCs for different values of v_d at the well during the pumping phase.

Fig.4 The schematic diagram of the flow system nearby well for the pumping phase.

Fig.5 Concentration distributions in a 2D horizontal plane at t_{pump}=0 hr. a) $v_d = 1\times10^{-6}$ m/s, b) $v_d = 1.5\times10^{-6}$m/s; c) $v_d = 2\times10^{-6}$ m/s; d) $v_d = 3\times10^{-6}$ m/s.

Fig.6 BTCs for different skin hydraulic conductivities at the well during the pumping with r_s=0.7 m, and δ=0.25, 0.5, 1, 1.5 and 2.

Fig.7 2D horizontal plane distributions of concentration with r_s=0.7 m at t_{pump}=0 hr. a) δ= 0.25; b) δ= 0.5; c) δ= 1; d) δ= 1.5; e) δ= 2.

Fig.8 Curves of concentration versus distance at t_{pump}=0 hr with δ= 0.25, 0.5, 1, 1.5 and 2.

Fig. 9 BTCs for different skin indexes δ at the well during the pumping phase with r_s=0 m, 0.3 m, and 0.7 m.

Fig.10 2D horizontal plane distributions of concentration for different skin indexes δ at t_{pump}=0 hr. a) r_s =0.7 m, δ=0.5; b) r_s =0.3 m, δ=0.5; c) r_s= 0 m; d) r_s =0.3 m, δ=2 m; e) r_s =0.7 m, δ=2.

Fig.11 Curves of concentration versus distance for different skin indexes δ at t_{pump}=0 hr with r_s=0 m, 0.3 m, and 0.7 m.

Fig.12 BTCs at the well fitted by the non-skin model for different skin indexes δ with r_s =0.3 m, δ= 0.25 and 2,

583 Table 1. The parameter values used in this study

Parameter name	Symbols	Values
Aquifer thickness (m)	B	10
Radius of well screen (m)	r_w	0.1
Density of groundwater(kg/m^3)	ρ	1000
Effective porosity of aquifer	θ	0.3
Hydraulic conductivity of aquifer (m/d)	K	8
Constant heads of S_1(m)	H_1	15.22, 15.44, 15.69, 15.65, ,15.87, 16.08, 16.30
Constant head of S_2 (m)	H_2	15.0
Regional groundwater Darcy velocities (m/s)	v_d	5×10^{-7}, 1×10^{-6}, 1.5×10^{-6}, 2×10^{-6}, 2.5×10^{-6}, 3×10^{-6}
Longitudinal dispersivities of aquifer (m)	α_L	0.1
Hydraulic conductivity of skin zone (m/d)	K_s	2, 4, 12, 16
Effective porosity of skin zone	θ_s	,0.24,0.27,0.33,0.36
Skin radius (m)	r_s	0.3, 0.7
Injection or pumping rate (m^3/d)	Q	15, 30
Mass flux per unit area (kg/(m^2 • s))	N_0	0.02765, 0.5529

Injection time (hr)	t_{inj}	6
Rest time (hr)	t_{res}	24
Pumping time (hr)	t_{pump}	48

584

585

586 Table 2. The relative tracer mass recovered by the end of each SWPP test

types	positive skin	positive skin	non-skin	negative skin	negative skin
	δ=0.5, r_s=0.7	δ=0.5, r_s =0.3		δ=2, r_s =0.3	δ=2, r_s =0.7
μ (%)	0.95	0.85	0.83	0.82	0.74

587

588

589

590 Table 3. Parameter estimated by SWPP test model without skin

	Real values used in the model with skin	Estimated by the model without skin	
		positive skin(δ=0.5)	negative skin(δ=2)
α_L (m)	α_L=0.1	14α_L	17α_L
θ(dimensionless)	θ=0.3	0.5θ	1.53θ
v_d (m/s)	v_d=3.0×10^{-6}	0.6v_d	1.47v_d

591

592

593

594

595

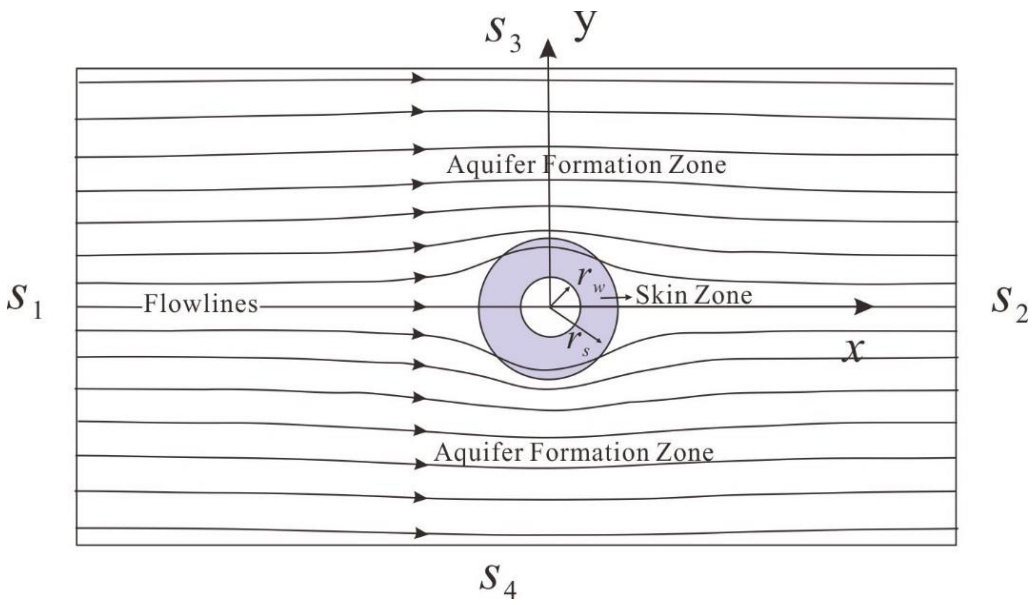

596

597

598

599

600 **Fig.1**

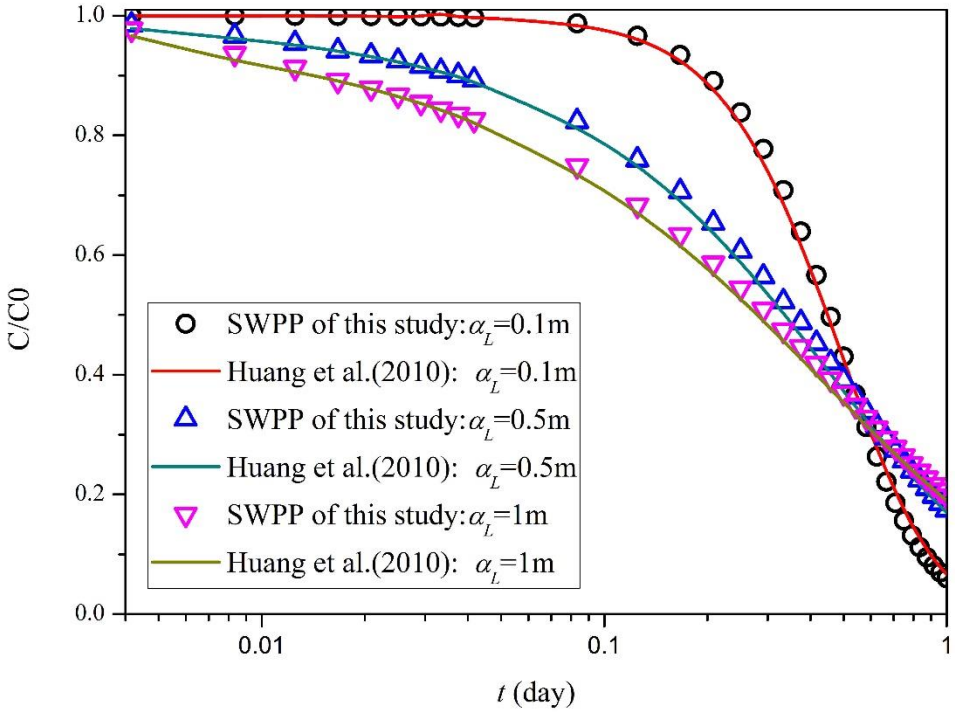

601

602

603

604

605

606 **Fig.2**

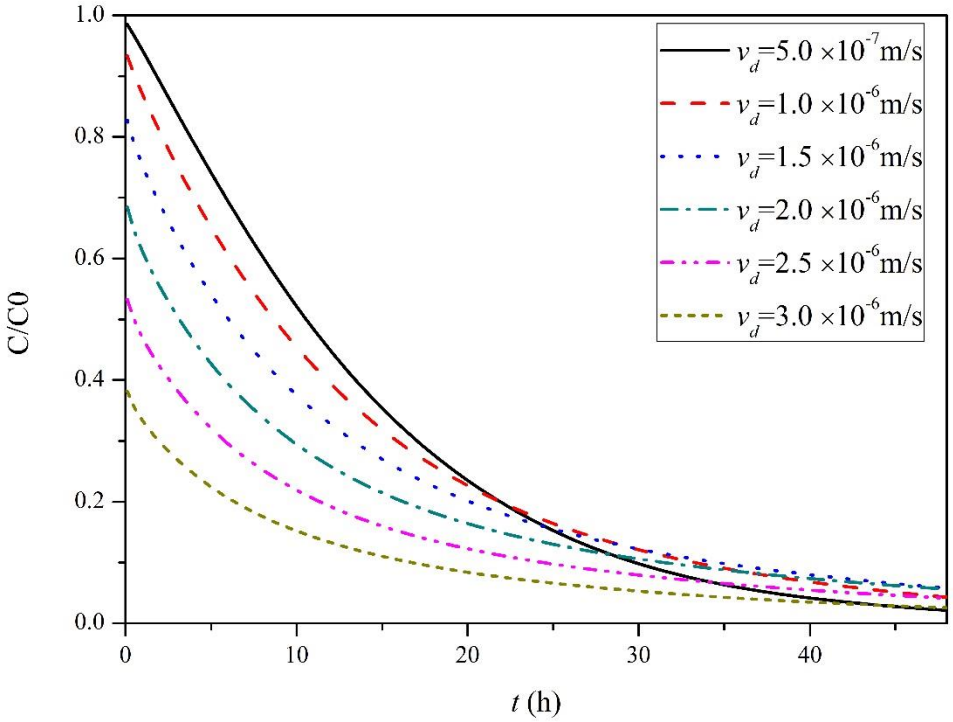

607

608

609

610

611 **Fig.3**

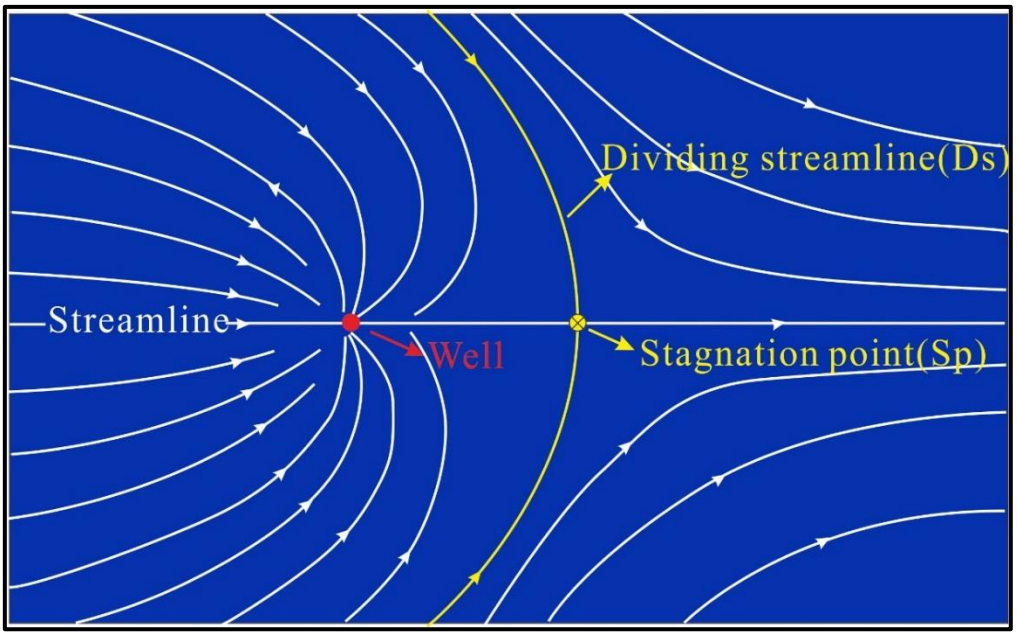

612

613

614

615

616

617

618 Fig.4

619

620 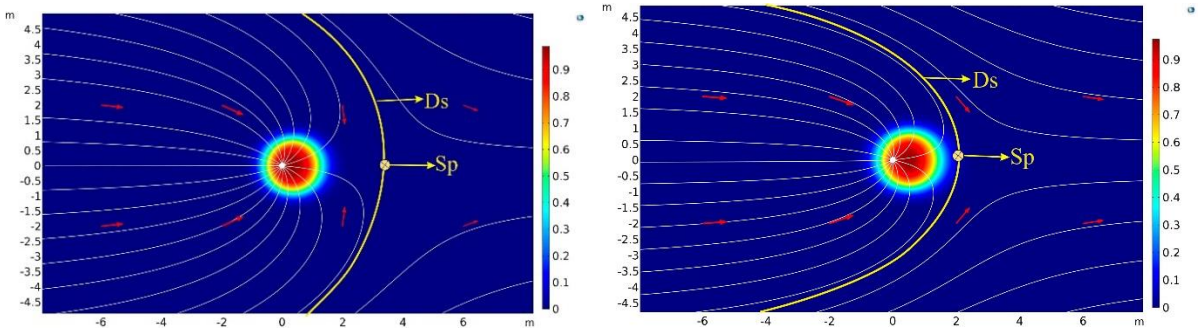

621 a. v_d=1e-6m/s b. v_d=1.5e-6m/s

622 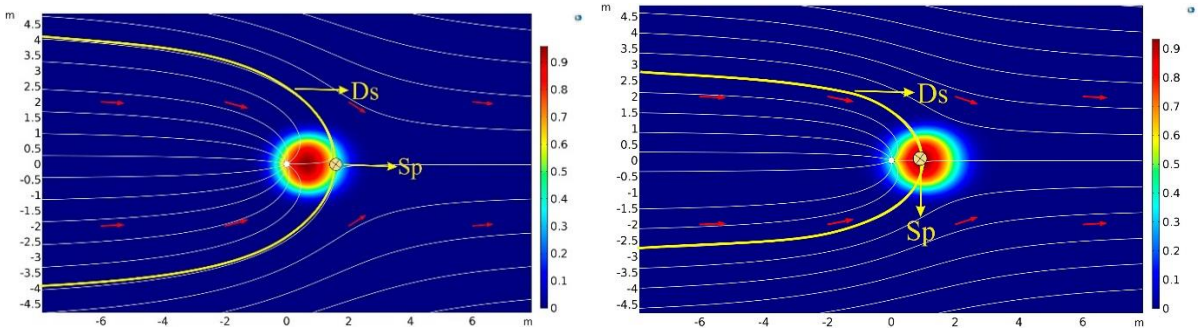

623 c. v_d=2e-6m/s d. v_d=3e-6m/s

624

625 **Fig.5**

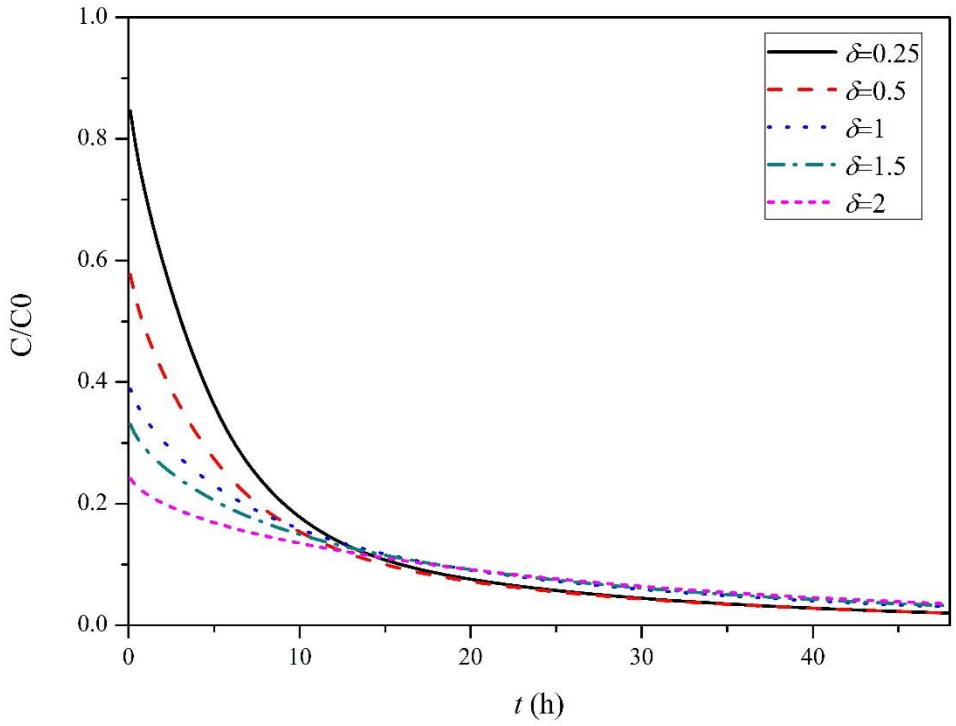

626

627

628

629

630 **Fig.6**

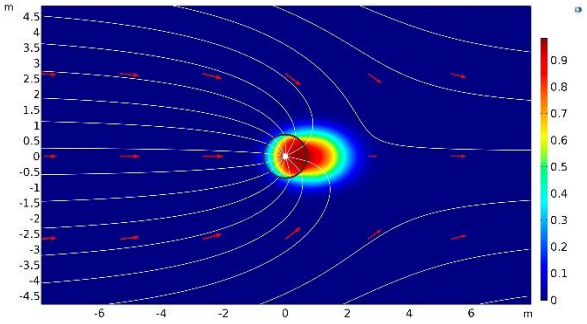

a. δ=0.25

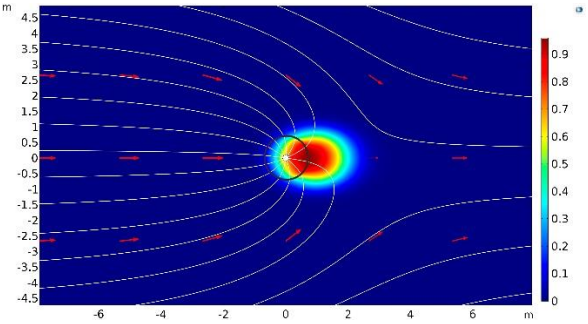

b. δ=0.5

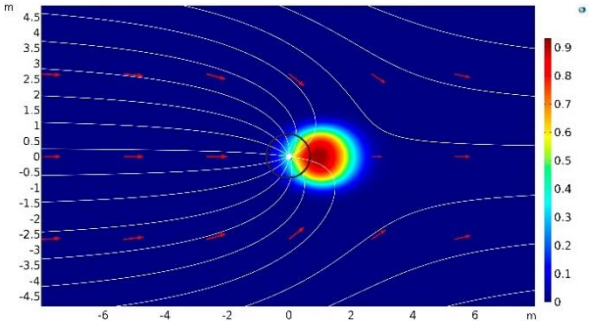

c. δ=1

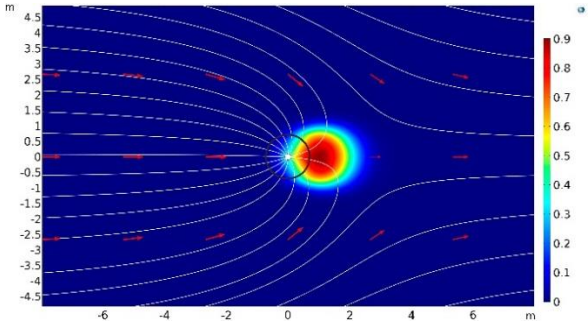

d. δ=1.5

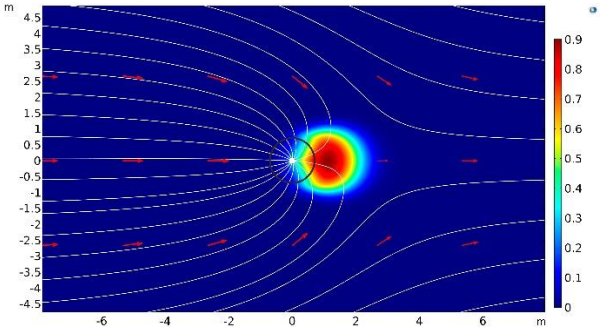

e. δ=2

Fig.7

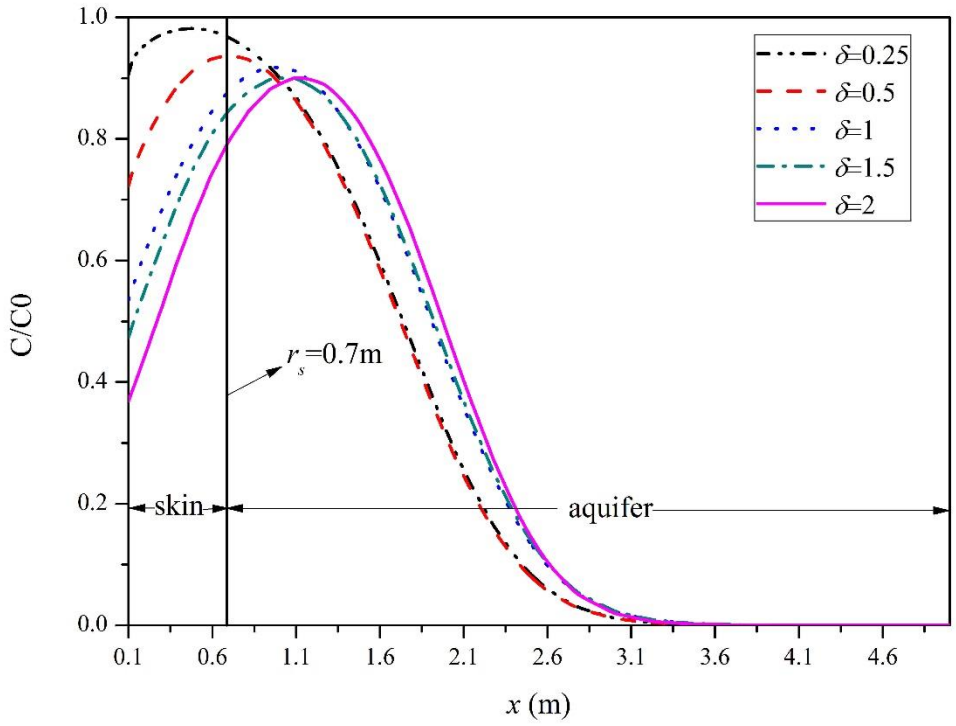

639

640

641

642

643 **Fig.8**

644

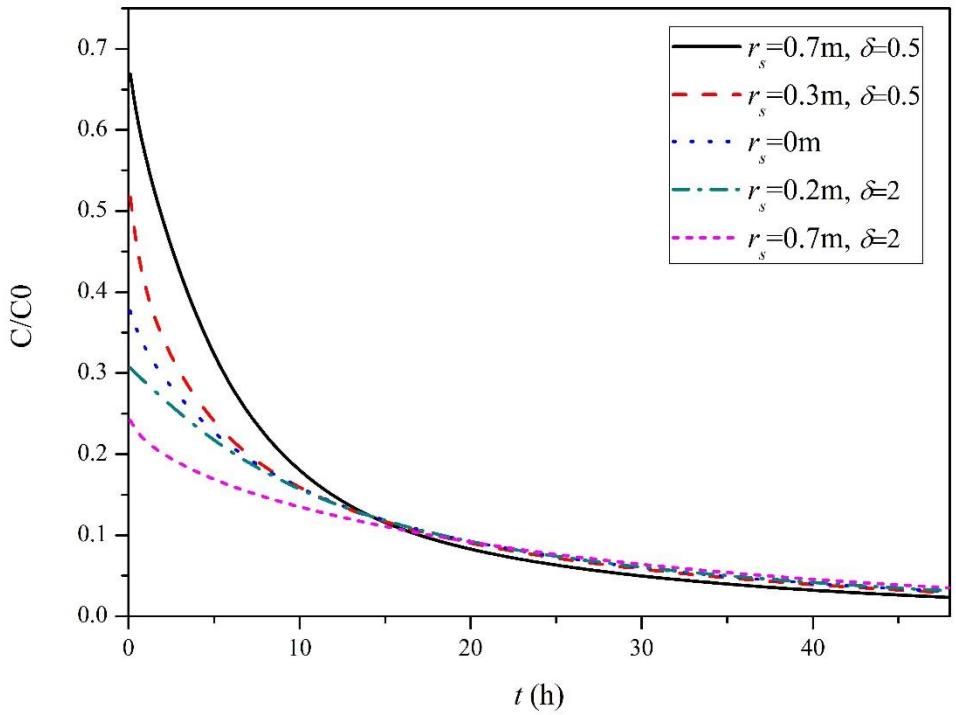

645

646

647

648

649

650 **Fig.9**

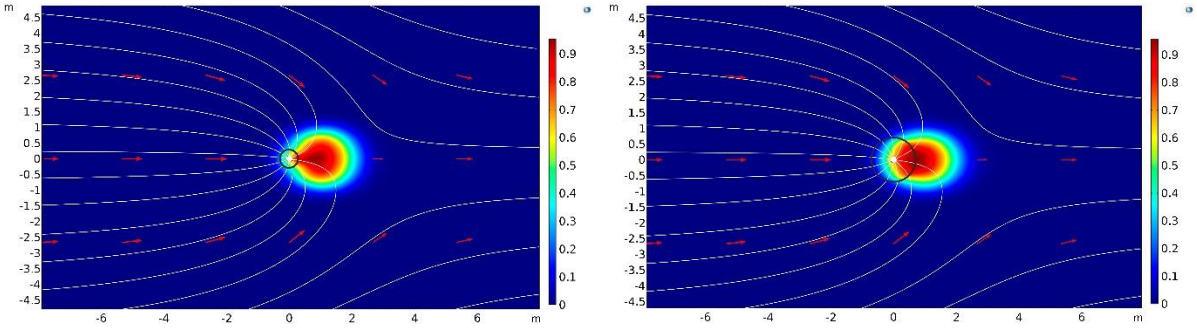

a. r_s =0.7 m, δ=0.5 b. r_s =0.3 m, δ=0.5

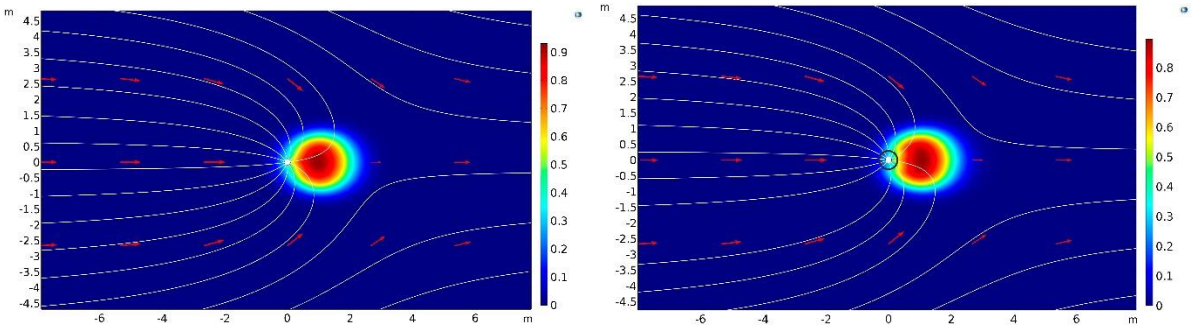

c. r_s =0 d. r_s =0.3 m, δ=2

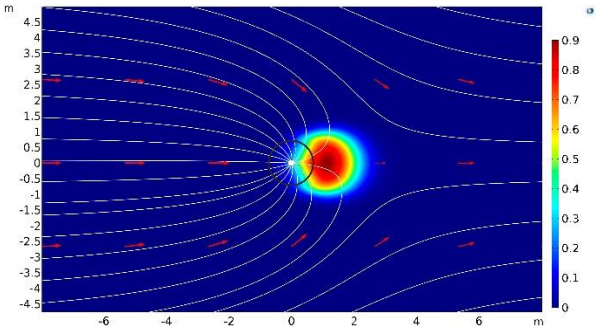

e. r_s =0.7 m, δ=2

Fig.10

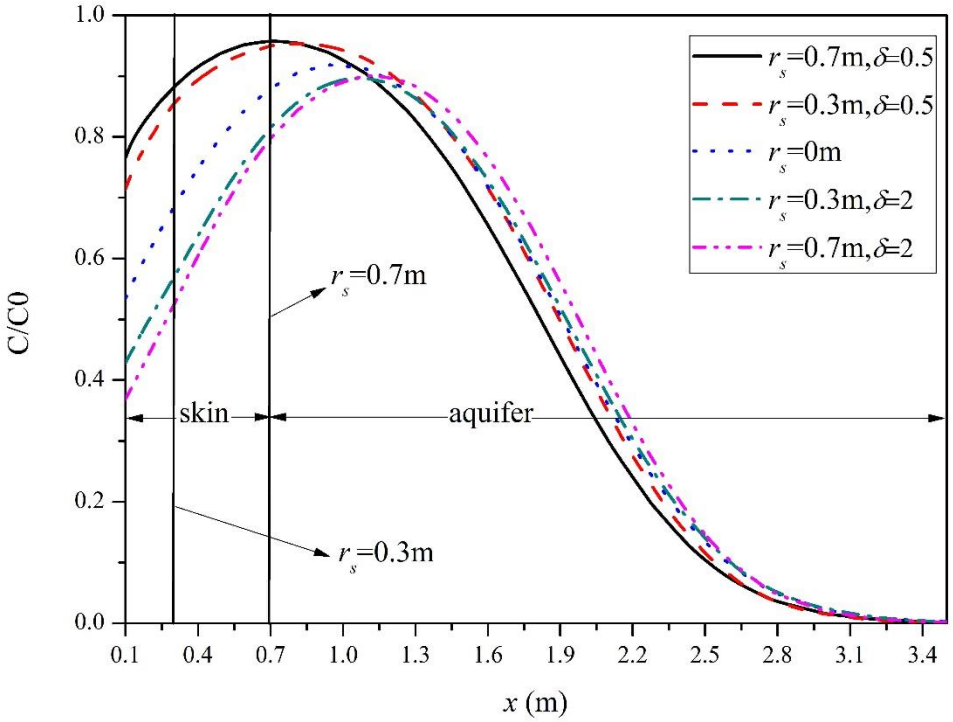

663

664

665

666

667

668 **Fig.11**

669

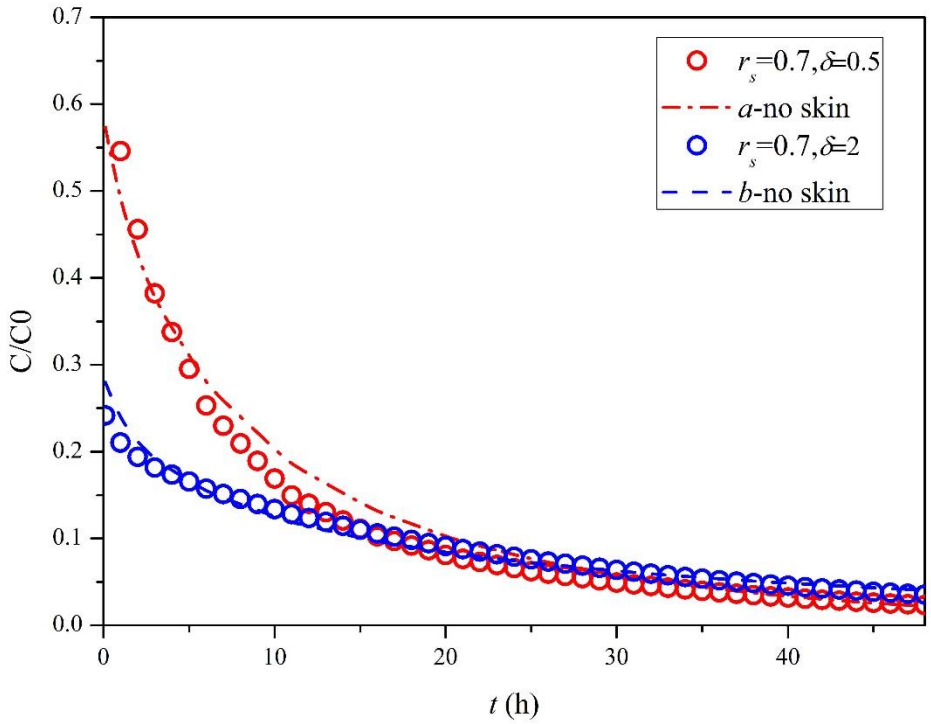

670

671

672

673

674 **Fig.12**

675

676

677

678

679

680

681